De La Torre-Paredes, C.; Domínguez-Berrocal, L.; Murguía, JR.; Marcos Martínez, MD.; Martínez-Máñez, R.; Bravo, J.; Sancenón Galarza, F. (02-2). epsilon-Polylysine-Capped Mesoporous Silica Nanoparticles as Carrier of the C9h Peptide to Induce Apoptosis in Cancer Cells. Chemistry - A European Journal. 24(8):1890-1897. https://doi.org/10.1002/chem.201704161

ε-polylysine-capped mesoporous silica nanoparticles as carrier of the C9h peptide to induce apoptosis in cancer cells

Cristina de la Torre,[a,b,c]† Leticia Domínguez-Berrocal,[d] † José R. Murguía,[a,b] M. Dolores Marcos,[a,b,c] Ramón Martínez-Máñez,[a,b,c]* Jerónimo Bravo,[d]* and Félix Sancenón[a,b,c]

Abstract: Apoptotic signalling pathways are altered in numerous pathologies such as cancer. In this scenario, caspase-9/PP2Acα interaction constitutes a key target with pharmacological interest to re-establish apoptosis in tumour cells. Very recently a short peptide (C9h) known to disrupt caspase-9/PP2Acα interaction with subsequent apoptosis induction was described. Here we prepared two sets of mesoporous silica nanoparticles loaded with safranin O (**S2**) or with C9h peptide (**S4**) and functionalized with ε-polylysine as capping unit. Aqueous suspensions of both nanoparticles showed negligible cargo release whereas in the presence of pronase a marked delivery of safranin O or C9h was observed. Confocal microscopy studies carried out with HeLa cells indicated that both materials were internalized and released their entrapped cargos. Besides, a marked decrease in HeLa cell viability (ca. 50%) was observed when treated with C9h-loaded **S4** nanoparticles. Moreover, **S4** provides peptide protection from degradation additionally allowing a dose reduction to observe an apoptotic effect when compared with C9h alone or in combination with a cell-penetrating peptide (i.e.Mut3DPT-C9h). Flow cytometry studies, by means of Annexin V-FITC staining, showed the activation of apoptotic pathways in HeLa as a consequence of **S4** internalization, release of C9h peptide and disruption of caspase-9/PP2Acα interaction.

Introduction

Apoptosis is a genetically programmed cell death that when deregulated is associated with cancers. Recently, several phosphatases have become attractive targets for the treatment of a variety of diseases, including cancers.[1-4] However, the only clinical drugs targeting phosphatases are the immunosuppressive cyclosporin A and FK506, which inhibit serine/threonine phosphatase 2B (calcineurin) and NFAT activation.[5-9] Nevertheless, long-term usage of these drugs can lead to undesirable side effects.[10]

Some of us previously generated a new bifunctional peptide that specifically binds PP2Acα (human DPT-C9h or mouse DPT-C9), composed by the cell-penetrating peptide (CPP) DPT-sh1 followed by a caspase-9-derived sequence (C9h).[11] The resulting sychnologic peptide targets caspase-9/PP2Acα interaction, leading to caspase-9 activation, mitochondrial membrane permeabilization, cytochrome c release and apoptosis in a variety of human and mouse cancer cell lines. The mouse-specific peptide DPT-C9 also induced tumor growth inhibition in lung (K-RasLA-1) and breast cancer (PolyomaMiddleT, PyMT) mouse models showing neither toxicity nor immunogenic response.[11] DPT-C9h had a specific effect on transformed B cells isolated from chronic lymphocytic leukemia patients without any effect on T-cells, NK-cells and monocytes, but did not show any effect on primary B cells from healthy donors.[12]

A major concern when using peptides as therapeutics is the potential effects of serum proteases on peptide degradation prior to cellular internalization. Several approaches have been used to stabilize CPPs for *in vivo* applications, such as the incubation with SDS or polysialic acid, substitution of L-aminoacids by D-isomers containing peptides, retroinversion, the use of non-natural aminoacids, modification of peptide backbones, cyclization, disulfide bond formation, constrained peptides and stapled peptides among others.[13] DPT-C9h serum proteolysis resistance was improved by mutating a serum protease cleavage site comprised within the CPP sequence. The peptide Mut3DPT-C9h with an arginine to alanine mutation at the eighth residue of the DPT sequence showed enhanced peptide stability and a better pharmacokinetic profile, also maintaining the same apoptotic effect as the original DPT-C9h.[14] However this and other reported techniques to stabilize peptides are complex and time consuming. In this scenario, we decided to explore alternative methods for delivering the caspase-9 derived sequence C9h in the cell in a CPP independent manner (*vide infra*).

From another point of view, the administration of certain drugs is hindered by their low water solubility, rapid degradation, decreased bioavailability and lack of specificity, which is responsible for severe side effects.[15,16] Such features highlight the limitations of certain drugs used nowadays in the clinic, since there are constraints relative to the maximum dose and number of treatments that can be administered to each patient.[17] In fact, such dose restriction in conjugation with a decreased bioavailability usually results in a lower therapeutic outcome and

[a] C. de la Torre, J. R. Murguía, M.D. Marcos, R. Martínez-Máñez, F. Sancenón
Instituto Interuniversitario de Investigación de Reconocimiento Molecular y Desarrollo Tecnológico (IDM), Universitat Politècnica de Valencia, Universitat de València, Valencia (Spain)
Camino de Vera s/n, 46022, Valencia (Spain).
E-mail: rmaez@qim.upv.es
[b] C. de la Torre, J. R. Murguía, R. Martínez-Máñez, F. Sancenón
CIBER de Bioingeniería, Biomateriales y Nanomedicina, Madrid (Spain).
[d] C. de la Torre, M. D. Marcos, R. Martínez-Máñez, F. Sancenón
Departamento de Química
Universidad Politécnica de Valencia, Valencia
Camino de Vera s/n, 46022, Valencia (Spain).
[d] L. Domínguez-Berrocal, J. Bravo
Departamento de Genómica y Proteómica
Instituto de Biomedicina de Valencia
c/ Jaime Roig 11, 46010, Valencia (Spain).
E-mail: jbravo@ibv.csic.es
† Both authors contributed equally to this work.

can trigger the development of resistance to these therapies.[18] Therefore, it is crucial to develop carriers capable of protecting drugs and delivering them in temporally controlled fashion, improving their therapeutic outcome as a result. Controlled release of drugs at will and at site is an expanding research field in biotechnology and biomedicine.[19]

In this scenario, the use of mesoporous silica nanoparticles (MSNs) as inorganic nanocarriers of selected cargo molecules (including drugs) has been extensively explored in the last decade due to favorable characteristics of MSNs such as large load capacity, biocompatibility, high thermal stability, homogeneous porosity, inertness and tunable pore sizes.[20-22] When compared to organic nanocarriers,[23] MSNs are more resistant to pH, temperature variations and to mechanical stress, which renders them an improved ability to protect the cargo when in contact with body fluids.[24] Drugs, genes or proteins are usually loaded in MSNs by submerging the nanoparticles in solutions containing the therapeutic molecules.[25] In this process, payloads are encapsulated in MSNs matrix by adsorption, a process that involves the formation of hydrogen bonds or electrostatic interactions between cargo molecules and MSNs. Besides, the external surface of the MSNs can be functionalized with certain molecular or supramolecular entities that controlled the release of the cargo at will upon the application of an external trigger.[26-28] These "gated" materials released the entrapped cargo in response to a local or external stimulus, such as pH, temperature, the presence of enzymes, electromagnetic field, near infrared (NIR) radiation, changes in redox potential, ultrasound and the presence of small molecules or biomolecules.[29] Gated materials have been extensively used in controlled release,[29a] in sensing/recognition protocols[30] and in complex communication networks.[31,32] Furthermore, MSNs have shown to preferentially accumulate in tumors in bio-distribution studies performed in human cancer xenograft models and effectively deliver drugs in tumors and suppress tumor growth, presenting a satisfactory biocompatibility.[33-35]

Several organic and inorganic carriers have been used to protect (from enzymatic degradation) and to deliver proteins and peptides. Several types of organic biocompatible polymers (in the forms of micro or nanoparticles), liposomes, micelles and carbon nanotubes have been used for this application.[36,37] In this scenario, MSNs have been used to encapsulate and deliver proteins[38-40] but its use as inorganic carriers for the controlled release of small peptides has been barely explored.[41]

Based in these concepts, we report herein the use of gated MSNs as nanocarriers to protect C9h from degradation and deliver the therapeutic peptide in cancer cells moreover allowing a dose reduction to observe an apoptotic effect.

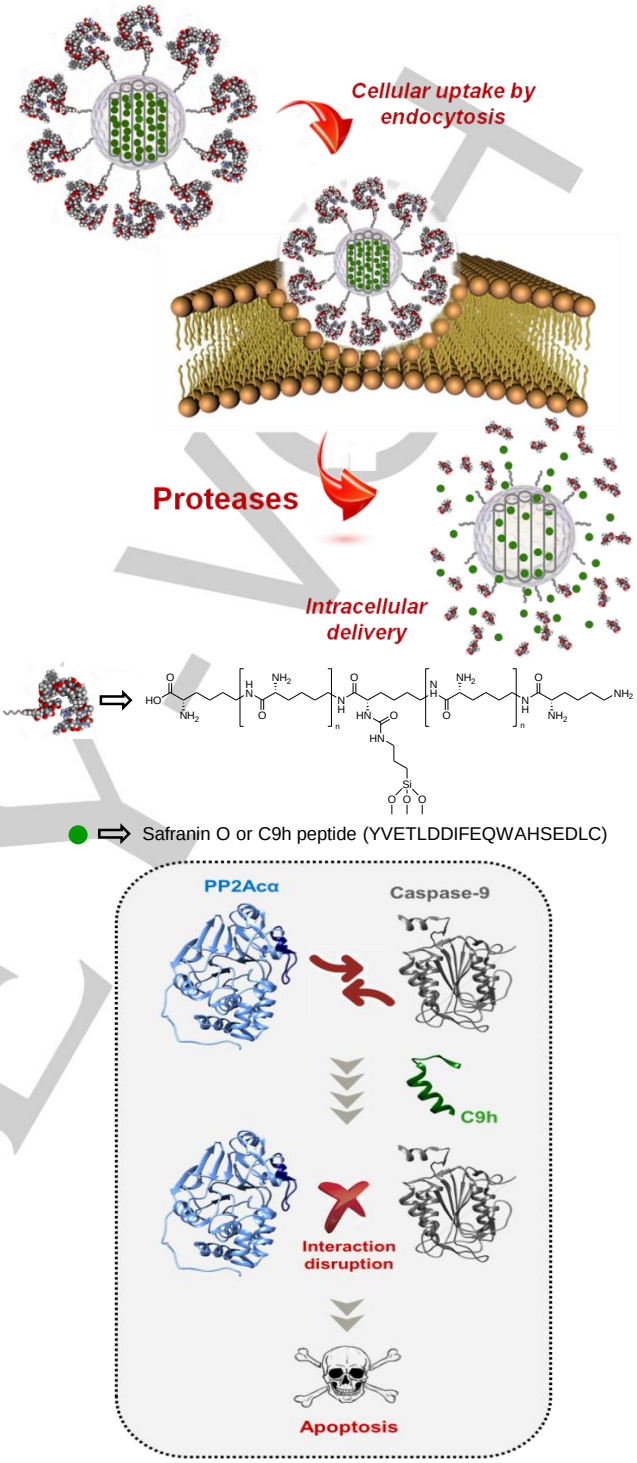

Scheme 1. Representation of the design and mechanism of action of MSNs **S4** loaded with C9h peptide in the presence of intracellular proteases (up) and mechanism of action of C9h blocking PP2Acα-caspase 9 interaction (down).

Results and Discussion

Synthesis and characterization of gated nanoparticles. A schematic representation of the designed nanoparticles is shown in Scheme 1. MSNs of ca. 100 nm diameter were selected as carriers. The support was loaded with safranin O or C9h peptide and the pores capped by the covalent grafting of ε-polylysine onto the external surface of the nanoparticles through the formation of urea bonds. In the presence of proteases, the ε-polylysine coating is expected to be hydrolyzed allowing cargo release in cells (see Scheme 1). Moreover, the intracellular release of the entrapped C9h peptide is expected to disrupt PP2Acα-caspase 9 interaction inducing apoptosis.

The ε-polylysine selected consists of 25–35 repeated units of the L-Lysine amino acid. Unlike normal peptide bonds, in which amino acids are linked through the amino group of the α-carbon, the lysine amino acids in ε-polylysine are molecularly linked by the amino moiety located in the ε carbon. This polymer is obtained by natural fermentation of *Streptomyces* bacterial strains.[42] ε-polylysine has been used as a drug-delivery and gene-delivery carrier in the development of hydrogels, and also as an antimicrobial agent.[43] In addition, it has been reported to be nontoxic for humans, even at high doses, and biodegradable by amidases.[44]

MSNs were synthesized using CTAB as a template and TEOS as a hydrolytic inorganic precursor.[45] Calcination of the mesostructured phase resulted in the starting porous scaffold (solid **S0**). Then the pores of **S0** were loaded with safranin O by suspending nanoparticles in an acetonitrile solution of the dye for 24h and the external surface was functionalized with (3-isocyanatopropyl)triethoxysilane yielding solid **S1**. Finally, ε-polylysine was covalently anchored onto the external surface through the formation of urea bonds to cap the pores (solid **S2**).[46]

Another set of nanoparticles were prepared, employing a similar procedure to that describe above, but using C9h peptide (YVETLDDIFEQWAHSEDLK) as cargo instead of safranin O. In a first step, the size of the C9h peptide was assessed using the data extracted from the Protein Data Bank (PDB), code 1JXQ in order to determine if C9h can be loaded in the pores of **S0**.[12] Scheme 2 shows the α-helix structure of the sequence corresponding to C9h in the caspase-9 crystallographic structure. As could be seen from the crystallographic data, the C9h peptide adopts a quasi-cylindrical shape with a diameter of ca. 1.7 nm and a length of ca. 2.25 nm. Taking into account that pore diameter of **S0** is 3.32 nm (see Table 1) it was expected that C9h could be loaded efficiently into the nanoparticles. However, it is known that peptide structure can vary as a function of the solvent used. Therefore, in a second study, a structure analysis of C9h peptide was performed by circular dichroism in PBS buffer. As could be seen in Figure 1, C9h peptide adopted a non-structured conformation in PBS, which was different than that shown by the same sequence in caspase 9. However, it was found that C9h adopted a helical conformation upon addition of increasing quantities of trifluoroethanol (TFE). When TFE content reached 40%, C9h showed two troughs of molar ellipticity at 208 and 222 nm, characteristics of a high content of α helix in the sample.[47]

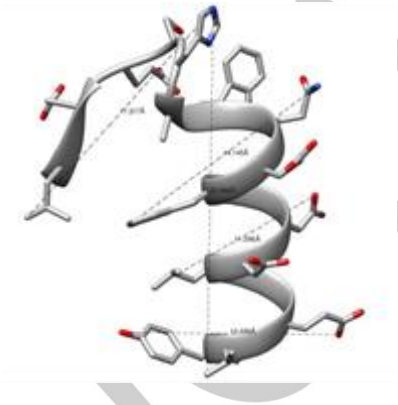

Scheme 2. Minimized structure of the peptide fragment, corresponding to C9h, inside caspase-9 protein.

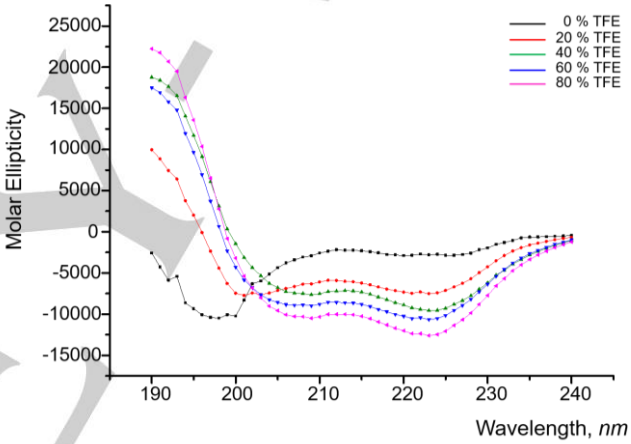

Figure 1. Circular dichroism spectra of C9h peptide in PBS buffer and in the presence of increasing quantities of TFE.

For the preparation of peptide loaded nanoparticles, solid **S0** was suspended in a solution containing C9h and the suspension was stirred for 24 h. The external surface of the C9h-loaded nanoparticles was then functionalized with 3-isocyanatopropyl)triethoxysilane yielding solid **S3** and afterwards, the pores were capped by the grafting of ε-polylysine through the formation of urea bonds (solid **S4**). Besides, we also prepared solid **S5** that is a similar solid to **S4** but loaded with C9h peptide labelled with rhodamine B (YVETLDDIFEQWAHSEDLK-RhB).

Solids **S0**, **S1** and **S2** were fully characterized by powder X-ray diffraction (PXRD), transmission electron microscopy (TEM), N_2 adsorption-desorption isotherms, thermogravimetric measurements, elemental analyses and dynamic light scattering (DLS). The X-ray pattern of as-made MSNs showed four mesoporous characteristic low-angle reflections of a hexagonal-

ordered array indexed as (100), (110), (200) and (210) Bragg peaks (see Supporting Information, Figure SI-1, curve a). Calcination of MCM-41 (solid **S0**) induced a significant shift of the (100) reflection (Figure SI-1, curve b). Finally, the subsequent loading steps with safranin O and further functionalization with ε-polylysine resulted in the loss of the (110) and (200) reflections, given the reduced contrast after loading/functionalization (Figure SI-1, curves c and d). However, the permanence of the (100) peak still indicated that the mesoporous structure was maintained in **S1** and **S2** nanoparticles. TEM images of **S0**, **S1**, **S2** and **S4** showed that solids were obtained as spherical nanoparticles with diameters in the 80-100 nm range (see Figure 2 and Supporting Information Figure SI-2).TEM images confirmed the preservation of the mesoporous structure in all prepared solids. Besides, the size of the nanoparticles was determined by DLS. As shown in Figure 3, diameters of 96, 116, 147 and 169 nm were determined for **S0**, **S1**, **S2** and **S4** nanoparticles, respectively.

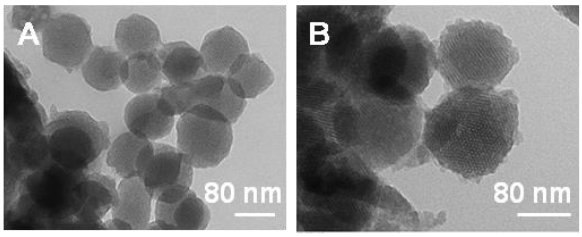

Figure 2. TEM images of (a) **S0** and (b) **S4**.

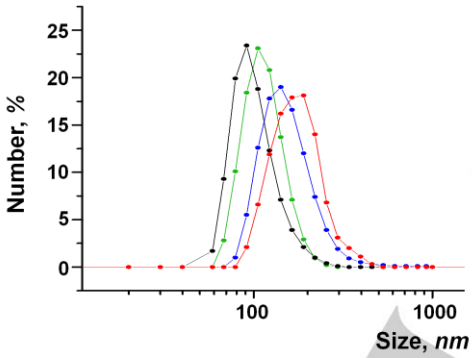

Figure 3. Size distribution by number of particles obtained by DLS studies for **S0** (black), **S1** (green), **S2** (blue) and **S4** (red) solids.

The N_2 adsorption-desorption isotherms of **S0** showed an adsorption step at intermediate P/P_0 value (0.1-0.3) which is related to the nitrogen condensation inside the mesopores by capillarity (see Supporting Information Figure SI-3). The application of the BET model resulted in a value for the total specific surface of 1101.2 $m^2\ g^{-1}$ and a pore volume of 1.17 $cm^3\ g^{-1}$. From the PXRD, porosimetry and TEM studies, the a_0 cell parameter (4.50 nm), the pore diameter (3.32 nm) and the value for the wall thickness (1.18 nm) were calculated. The N_2 adsorption-desorption isotherms of **S1** and **S2** nanoparticles were typical of mesoporous systems with filled mesopores (see Figure SI-3), and a significant decrease in the N_2 volume adsorbed and in the specific surface area was observed (278.7 $m^2\ g^{-1}$ and 111.4 $m^2\ g^{-1}$ for **S1** and **S2**, respectively). BET specific surface values, pore volumes and pore sizes calculated from the N_2 adsorption-desorption isotherms for **S0**, **S1** and **S2** are listed in Table 1.

Table 1. BET specific surface values, pore volumes and pore sizes calculated from the N_2 adsorption-desorption isotherms for selected materials.

Solid	S_{BET} [$m^2\ g^{-1}$]	Pore size[a,b] [nm]	Pore volume[a] [$cm^3\ g^{-1}$]
S0	1101.2	3.32	1.17
S1	278.7	-	0.41
S2	111.4	-	0.24

[a] Pore volumes and pore sizes are only associated with intraparticle mesopores.
[b] Pore size estimated by using the BJH model applied on the adsorption branch of the isotherm.

Table 2. Content of the molecular gate and guest molecules in grams per gram of SiO_2 for **S2** and **S4** nanoparticles.

Solid	α guest molecule [$g/g^{-1}\ SiO_2$]	α gate [$mmol/g^{-1}\ SiO_2$]
S2	0.02	0.08
S4	0.02	0.02

Safranin O, C9h peptide and ε-polylysine contents in **S2** and **S4** nanoparticles were determined by elemental analysis and thermogravimetric studies and are showed in Table 2.

Cargo release studies of the capped nanoparticles. Cargo delivery from **S2** and **S4** was tested in the absence and in the presence of pronase from *Streptomyces griseus*. In a typical experiment, **S2** and **S4** nanoparticles were suspended in water at pH 8.0 at a final concentration of 0.5 mg mL^{-1}. The suspensions were stirred at 37ºC in the absence and in the presence of pronase. Uncapping and subsequent delivery of the dye from **S2** was determined through the measurement of fluorescence emission at 585 nm (λ_{ex} = 525 nm) of released safranin O at scheduled times. For solid **S4**, C9h peptide delivery was quantified through its absorbance at 280 nm. The obtained delivery profiles from **S2** and **S4** are shown in Figure 4. A negligible safranin O release from **S2** in the absence of pronase was observed (ca. 5% of the maximum dye delivered after 24 h). In contrast, a marked dye delivery was found in the presence of enzyme. A similar trend was observed for solid **S4** loaded with C9h peptide (Figure 4B); i.e. payload delivery was only found in the presence of pronase whereas a poor cargo

release was observed in the absence of the enzyme. These results demonstrated that both rhodamine B dye and C9h peptide can be encapsulated in MSNs and delivered on-command in the presence of pronase.

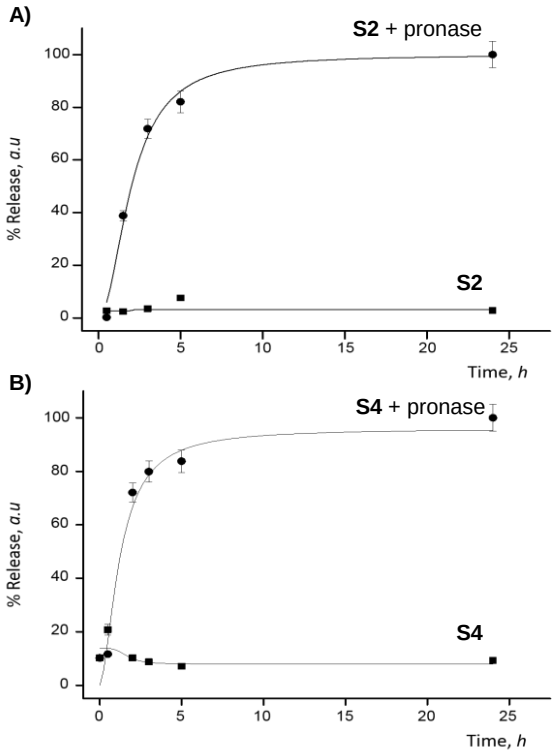

Figure 4. Release profiles of safranin O (A) and C9h peptide (B) from solids **S2** and **S4** in the absence and in the presence of pronase enzyme. Both data sets were collected at 25ºC.

Cellular studies. Once the specific cargo release was proven, controlled payload delivery of **S2**, **S4** and **S5** nanoparticles was tested using HeLa cells. In a first step, **S2** and **S5** uptake and cargo release in HeLa cells was studied by confocal microscopy. Cells were also stained with the DNA marker Hoechst 33342. The obtained results are shown in Figure 5. As could be seen, a marked cytoplasmic fluorescence associated with safranin O was observed for HeLa cells treated with **S2** nanoparticles. This observed fluorescence was ascribed to a proper uptake of **S2** nanoparticles by cells with subsequent hydrolysis of the ε-polylysine caps in lysosomes and safranin O intracellular delivery. Nearly the same results were obtained using **S5** nanoparticles. This solid was also successfully uptake by HeLa cells and the rhodamine B-labelled C9h peptide intracellularly delivered (Figure 5).

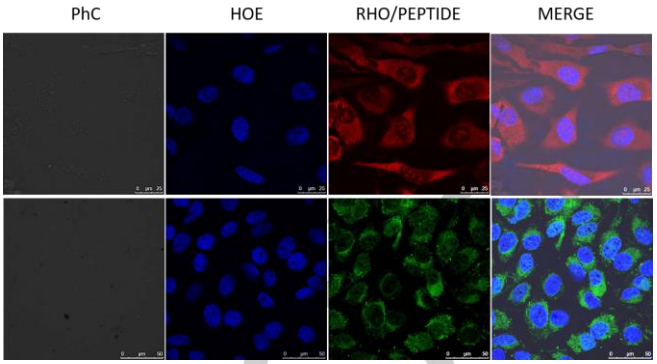

Figure 5. Confocal microscopy images of HeLa cells treated with 50 μg mL^{-1} of **S2** and **S5** nanoparticles. The cellular uptake was followed by safranin O associated fluorescence (red) or rhodamine B-peptide associated fluorescence (green) in the presence of DNA marker Hoescht 33342 (blue).

In a second step, and in order to discard any toxicity associated with the mesoporous scaffold or the ε-polylysine coating shell, cell viability assays using the safranin O-loaded solid **S2** at different concentrations were evaluated by the WST-1 test (see Figure 6). As could be seen **S2** nanoparticles were non-toxic for HeLa cells at concentration up to 500 μg mL^{-1} after 24 h of incubation.

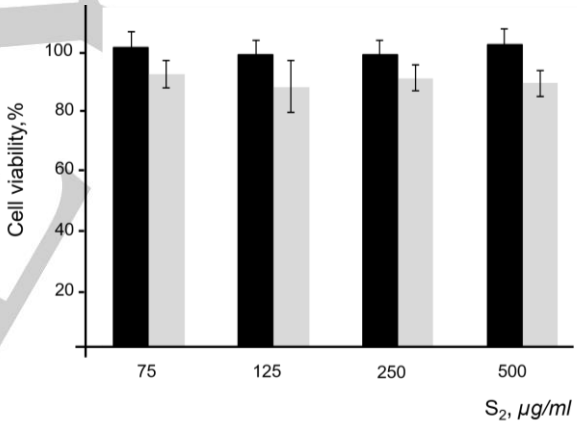

Figure 6. WST-1 viability assays carried out with different concentrations of **S2** nanoparticles incubated 24 (black bars) and 72 h (grey bars) and with HeLa cells. These measurements were carried out at 37ºC.

After demonstrating that the MSNs are not toxic the apoptotic effect of C9h peptide delivered by **S4** in HeLa cells was studied. For this purpose HeLa cells were treated with three different concentrations of **S4** nanoparticles (75, 125 and 250 μg mL^{-1}) and cell viability was determined at 24, 48 and 72 h of incubation. Moreover, equivalent concentrations of Mut3DPT-C9h (1.35, 2.70 and 5.40 μM) to the concentrations of peptide delivered by **S4** were also analyzed in the same experimental conditions as controls. The obtained results are shown in Figure

7. From the data it can be concluded that C9h peptide delivered from **S4** nanoparticles after 72 h of incubation induced a sharp decrease in cell viability at 125 and 250 μg mL^{-1}. Also, cell viability reduction induced by C9h delivered from **S4** showed to be higher than that obtained using Mut3DPT-C9h at equivalent amounts (5.40 μM and 2.70 μM of peptide). At these concentrations, Mut3DPT-C9h was able to induce only a 10-20% decrease in cell viability, whereas when encapsulated in **S4** a marked 50% reduction was observed.

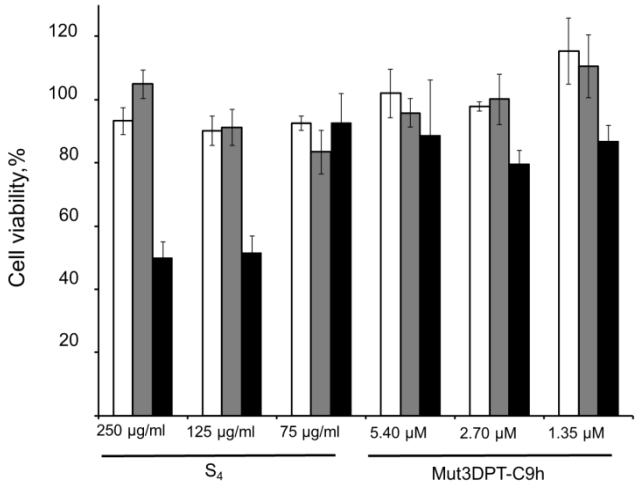

Figure 7. WST-1 cell viability assay of HeLa cells treated with **S4** (75, 125 and 250 μg mL^{-1}) and with Mut3DPT-C9h (1.35, 2.70 and 5.40 μM) for 24 (white bars), 48 (grey bars) and 72 h (black bars). 250, 125 and 75 μg mL^{-1} of **S4** corresponds to 5.40, 2.70 and 1.35 μM of Mut3DPT-C9h, respectively. These experiments were carried out at 37ºC.

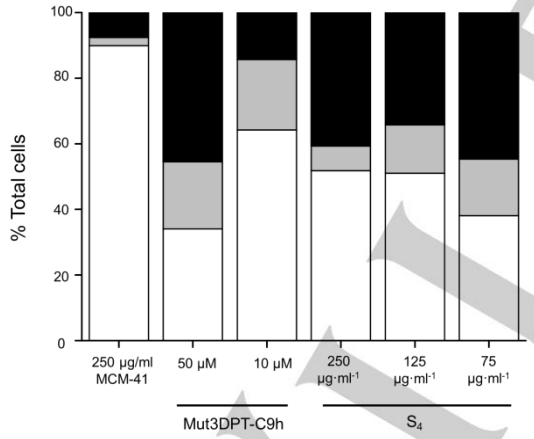

Figure 8. Quantification of cell viability and cell death was performed by flow cytometry by means of Annexin V-FITC staining. The percentage of dead cells (black), cells undergoing cell death (gray), and healthy cells (white) are shown for a 75, 125 and 250 μg mL^{-1} concentration of **S4** and as positive control were used Mut3DPT-C9h peptide at 10 μM and 50 μM. These experiments were carried out at 37ºC.

Finally, in order to get a better characterization of the apoptotic effect of C9h delivered from **S4**, apoptosis induction was measured using AnnexinV-FITC detection kit and analyzed by flow cytometry. For this purpose, HeLa cells were incubated with **S4** (at concentrations of 75, 125 and 250 μg mL^{-1} that corresponds to 1.35, 2.70 and 5.40 μM of free Mut3DPT-C9h, respectively) and Mut3DPT-C9h (10 and 50 μM). Cells treated with 50 μM of Mut3DPT-C9h were used as positive control. As could be seen in Figure 8, treatment of HeLa cells with 10 μM Mut3DPT-C9h induced a 36% of apoptosis, while a peptide concentration of 1.35 μM encapsulated in **S4** (75 μg mL^{-1} of **S4**) induced ca. 55 % of cell death. A similar cell death was found for 50 μM of Mut3DPT-C9h and 75, 125 and 250 μg mL^{-1} of **S4**. Therefore, nanoformulation of DPT-C9h enhanced 37-fold the apoptotic effect of the peptide free in solution.

Mut3DPT-C9h is an improved variant of the original DPT-C9h CPP that has increased stability in mouse serum while keeping the same pro-apoptotic properties.[2] However, cancer cells treated with the therapeutic peptide C9h without being coupled to a delivery system at concentrations as high as 100 μM showed the same apoptosis levels as non-treated cells, since this peptide is not capable of being internalized in the cells without a vehicle.[1] Despite the reported advantages for cargo delivery into the cells, CPPs suffer some shortcomings as pharmaceutical products such as short duration of action caused by proteolysis and rapid renal clearance.[48] The results obtained with **S4** nanoparticles are remarkable because (i) allow the use of the C9h peptide without any modification and (ii) permit a peptide dose reduction up to 37 times to induce apoptosis in cancer cells.

Frequently, high biodegradability and low bioavailability have been limiting obstacles for the therapeutic use of peptides. Blood plasma contains more than 120 proteins, among which are present numerous proteolytic enzymes involved in peptide degradation. Our approach, i.e. peptide encapsulation in gated MSNs, could be of general application to deliver peptides. This may be of importance taking into account that a large number of peptide therapeutics has not obtained FDA approval as they have been considered poor drug candidates because of their low bioavailability and instability.

Conclusions

In summary, we report herein the synthesis and characterization of two gated nanoparticles loaded with safranin O and with C9h peptide. Both materials are based in the use of MSNs as carriers and capped with ε-poylysine as a pronase-triggered biomolecular gate. Both nanoparticles showed negligible cargo release in the absence of pronase, whereas in the presence of enzyme a remarkable payload delivery was observed due the enzyme-induced ε-poylysine hydrolysis. Confocal microscopy studies revealed that HeLa cells were able to uptake both nanoparticles with subsequent cargo delivery. Moreover, **S4** nanoparticles (loaded with C9h) induced a marked reduction in HeLa cells viability as the peptide delivered

promoted cell apoptosis. **S4**, or similar nanodevices based on MSNs, could be an alternative for C9h delivery inside cells without any sequence modification (such as the use of CPPs). Moreover, **S4** provides peptide protection from degradation additionally allowing a dose reduction of up to ten times to observe an apoptotic effect when compared with C9h alone or in combination with a CPP (i.e.Mut3DPT-C9h).

Experimental Section

Chemicals: Tetraethylorthosilicate (TEOS), *n*-cetyltrimethylammonium bromide (CTAB), sodium hydroxide, safranin O, 3-(triethoxysilyl)propyl isocyanate and the protease enzyme from *S. griseus* were purchased from Sigma–Aldrich Quimica S.A. (Madrid, Spain) and were used without further purification. ε-Poly-L-lysine was purchased from Chengdu Jinkai Biology Engineering Co., Ltd. All the other reagents were of a general laboratory grade and were purchased from Merck, unless otherwise specified. For cell culture studies, DMEM with high glucose, phosphate buffer, foetal bovine serum (FBS), trypsin and Hoescht 33342 were provided by Gibco. Cell proliferation reagent (WST-1) was obtained from Roche Applied Science. Annexin V-FITC was supplied by BD.

General techniques: PXRD, TG analysis, elemental analysis, EDX microscopy, N_2 adsorption-desorption isotherms were used to characterize the prepared materials. Power X-ray measurements were performed on a Philips D8 Advance diffractometers using CuKα radiation. Thermogravimetric analysis were carried out on a TGA/SDTA 851e Mettler Toledo balance, using an oxidant atmosphere (air, 80 ml/min) with a heating program consisting on a heating ramp of 10ºC per minute from 393 to 1273 K and an isothermal heating step at this temperature during 30 minutes. Elemental analysis was performed in a CE instrument EA-1110 CHN Elemental Analyzer. TEM images were obtained with a 100 kV JEOL JEM-1010 microscope. Nitrogen adsorption-desorption isotherms were recorded on a Micromeritics ASAP2010 automated sorption analyzer. Samples were degassed at 120ºC in a vacuum system overnight. Specific surface areas were calculated from the adsorption data in the low pressure range using the Brunauer-Emmett-Teller (BET) theory model. Pore size was determined following the Barrett-Joyner-Halenda (BJH) method. Fluorescence spectroscopy was carried out on a Felix 32 Analysis 1.2.

Synthesis of S0: CTAB (1.00 g, 2.74 mmol) was first dissolved in 480 mL of deionized water. After that, NaOH (3.5 mL, 2 M) in deionized water was added to the CTAB solution and the temperature was adjusted to 80ºC. TEOS (5 mL, 2.57 x 10^{-2} mol) was then added dropwise to the surfactant solution. The mixture was stirred for 2 h to yield a white precipitate. Finally the solid product was centrifuged, washed with deionized water and ethanol and dried at 60ºC. To prepare the final porous scaffold (**S0**), the as-made solid was calcined at 550ºC using an oxidant atmosphere for 5 h to remove the template phase (CTAB).

Peptide synthesis: Peptide C9h was synthesized by Synpeptide, adding an extra cysteine residue at the C-terminal to allow quantification. Peptide C9h-rhodamine B was synthesized by Synpeptide labeled with rhodamine B at the C-terminal.

Synthesis of S1, S2, S3 and S4: S0 nanoparticles (30 mg) were suspended in a solution of acetonitrile (5 mL) containing safranin O (20 mg) or in a solution of DMSO (5 mL) containing C9h peptide (18 mg). Both mixtures were stirred overnight at room temperature. Afterward, excess of 3-(triethoxysilyl)propylisocyanate (60 µL, 0.2 mmol) was added and the final crudes stirred for 5.5 h at room temperature. By this procedure we obtained **S1** (loaded with safranin O) and **S3** (loaded with C9h peptide). Then, ε-polylysine (30 mg, 6.0 x 10^{-3} mmol of polymer) dissolved in acetonitrile (5 mL) was added to the previous suspensions and stirred for 2 h. Finally, the solids were filtered off. Once dried, both solids were washed with methanol to remove the unreacted ε-polylysine and then with PBS to remove the cargo remaining outside the pores. Finally, the solids were filtered and dried at vacuum. This experimental procedure yielded the final solids **S2** (loaded with safranin O) and **S4** (loaded with C9h peptide).

Synthesis of S5: Solid **S5** was prepared following the same procedure described above for **S2** and **S4** but loading nanoparticles with C9h peptide derivatized with rhodamine B (YVETLDDIFEQWAHSEDLK-RhB).

Circular dichroism: 50 µM of C9h peptide was dissolved in 10 mM sodium phosphate buffer pH 7.65. Samples were prepared in a final volume of 300 µL of 10 mM sodium phosphate buffer pH 7.65 with increasing concentrations of trifluoroethanol (20%, 40%, 60% and 80%). Samples were introduced in the spectropolarimeter in a quartz Suprasil Precission cell 0.1 cm cuvette (Hellma), using 300 µL of buffer solution as blank. Measurements were performed at 20ºC and repeated 10 times for each sample and 5 times for each blank. Spectropolarimeter raw data were generated in millidegrees and further corrected by substracting blank value to sample value and further converted to molar ellipticity units with Jasco software.

Cell culture: HeLa cells were cultured in DMEM supplemented with 10% FBS at 37ºC with 5% CO_2 and underwent passage twice a week.

WST-1 cell viability assay: Cells were cultured in 24-well microtiter plates at a density of 25 x 10^3 cells/well and allowed to attach for 24 h. **S2** was added to the cells at a final concentration from 75 to 500 µg mL^{-1}. After 24h of incubation, 10 µL of WST-1 were added to each well and incubated for 90 minutes. **S4** was added to the cells at a final concentration of 250, 125 and 75 µg mL^{-1} and incubated for 24, 48 and 72 h. Cell viability was measured with WST-1 reagent and absorbance at 450 and 690 nm as reference wavelength was measured with a Wallac 1420 workstation.

Confocal microscopy cellular internalization assays: HeLa cells were seeded in six-well microtiter plates at a density of 1.5 x 10^5 cells/well. After 24 h, cells were treated with 50 µg mL^{-1} of **S2**. After 30 min, medium was removed and cells were washed with PBS. Then, cells were incubated for 20 h at 37ºC and visualized under a confocal microscope.

FACS Annexin V apoptosis measurements: 25000 HeLa cells in 1 mL of DMEM supplemented with 10% FBS per well were seeded in 24-well plates and incubated for 24h at 37ºC with 5% CO_2 before being treated with different concentrations of **S4** and the equivalent concentration of Mut3DPT-C9h. Cells treated with 1% DMSO were used as negative control. After 24 h of incubation, AnnexinV – FITC apoptosis detection kit was added to the samples following the manufacturer's protocol and samples were analyzed with a FACS Canto (BD) flow cytometer.

Acknowledgements

The authors wish to express their gratitude to the Spanish government (Projects MAT2015-64139-C4-1, SAF2012-31405, SAF2015-67077-R, AGL2015-70235-C2-2-R (MINECO/FEDER)), the Generalitat Valencia (Projects PROMETEOII/2014/047, PROMETEO/2012/061) and the CIBER-BBN for their support. C.T. is grateful to the Spanish Ministry of Science and Innovation for her PhD fellowship.

Keywords: gated nanoparticles • apoptosis • caspase-9 • peptides • drug delivery

References

[1] M. A. Lyon, A. P. Ducrue, P. Wipf, J. S. Lazo, *Nat. Rev. Drug. Discov.* **2002**, *1*, 9612-9760.

[2] F. Ducret, C. Turc-Baron, P. Pointet, G. Vernin, O. Skowron, B. Mc Gregor, J. M. Gasc, G. Beaune, M. Vincent, *Nephrol. Ther.* **2005**, *1*, 52-61.

[3] D. F.Lazar, A. R. Saltiel, *Nat. Rev. Drug Discov.* **2006***, 5*, 333-342.

[4] N. K. Tonks, *Nat. Rev. Mol. Cell. Biol*. **2006**, *7*, 833-846.

[5] J. Liu, J. D. Farmer, W. S. Lane, J. Friedman, I. Weissman, S. L.Schreiber, *Cell.* **1991**, *66*, 807-815.

[6] Y. M. Li, J. E. Casida, *Proc. Natl. Acad. Sci. U.S.A.* **1992**, *89*, 11867-11870.

[7] R. E. Honkanen, *FEBS Lett.* **1993**, *330*, 283-286.

[8] A. H. Walsh, A. Cheng, R. E. Honkanen, *FEBS Lett*. **1997,** *416*, 230-234.

[9] H. Medyouf, H.Alcalde, C. Berthier, M. C. Guillemin, N. R. dos Santos, A. Janin, D. Decaudin, H. De Thé, *J.Ghysdael, Nat. Med.* **2007**, *6*, 736-741.

[10] S. Martinez-Martinez, J. M. Redondo, *Curr. Med. Chem.* **2004**, *11*, 9972-10070.

[11] I. Arrouss, F. Nemati, F. Roncal, M. Wislez, K. Dorgham, D. Vallerand, N. Rabbe, N. Karboul, F. Carlotti, J. Bravo, D. Mazier, D. Decaudin, A. Rebollo, *PLoS One* **2013**, *8*, e60816.

[12] I. Arrouss, D. Decaudin, S. Choquet, N. Azar, C. Parizot, J. M. Zini, F. Nemati, A. Rebollo, *Protein Pept. Lett*. **2015**, *22*, 539–546.

[13] J. Fominaya, J. Bravo, A. Rebollo, *Ther. Deliv*. **2015**, *6*, 1171-1194.

[14] J. Fominaya, J. Bravo, D. Decaudin, J. Y. Brossa, F. Nemati, A. Rebollo, *Ther. Deliv*. **2015**, *6*, 139–147.

[15] A. J. Primeau, A. Rendon, D. Hedley, L. Lilge, I. F. Tannock, *Clin. Cancer Res*. **2005**, *11*, 8782-8788.

[16] M. A. Izquierdo, R. H. Shoemaker, M. J. Flens, G. L. Scheffer, L. Wu, T. R. Prather, R. J. Scheper, *Int. J. Cancer* **1996**, *65*, 230-237.

[17] X. J. Liang, C. Chen, Y.Zhao, P. C. Wang, *Methods Mol. Biol.* **2010**, *596*, 467–488.

[18] Q. He, J. Shi, *Adv. Mater*. **2013**, *26*, 391–411.

[19] (a) C. Ding, Z. Li, *Mat. Eng. Sci. C* **2017**, *76*, 1440-1456; (b) A. Llopis-Lorente, B. Lozano-Torres, A. Bernardos, R. Martínez-Máñez, F. Sancenón, *J. Mater. Chem. B* **2017**, *5*, 3069-3083; (c) M. W. Tibbitt, J. E. Dahlman, R. Langer, *J. Am. Chem. Soc.* **2016**, *138*, 704-717.

[20] W. X. Mai, H.Meng, *Integr. Biol.*, **2013**, *5*, 19-28.

[21] A. L. Doadrio, A. J. Salinas, J. M. Sánchez-Montero, M. Vallet-Regí, *Curr. Pharm. Des.* **2015**, *21*, 6213-6819.

[22] C. Argyo, V. Weiss, C. Braüchle, T. Bein, *Chem. Mater,* **2014**, *26*, 435-451.

[23] (a) M. Gagliardi, C. Borri, *Curr. Pharm. Des.* **2017**, *23*, 393-410; (b) R. X. Zhang, T. Ahmed, L. Li, L. Yi, A. A. Z. Jason, X. Y. Wu, *Nanoscale* **2017**, *9*, 1334-1355; (c) X. Guo, L. Wang, X. Wei, S. Zhou, *J. Polym. Sci. A Polym. Chem.* **2016**, *54*, 3525-3550.

[24] Z. Li, J. C.Barnes, A. Bosoy, J. F.Stoddart, J. I. Zink, *Chem. Soc. Rev.* **2012**, *41,* 2590-2605.

[25] Y. Wang, Q. F. Zhao, N. Han, L. Bai, J. Li, J. Liu, E. X. Che, L. Hu, Q. Zhang, T. Y. Jiang, S. L. Wang, *Nanomed*. **2015**, *11*, 313-327.

[26] R. Sun, W. Wang, Y. Wen, X. Zhang, *Nanomat.* **2015**, *5*, 2019–2053.

[27] S. Mura, J. Nicolas, P. Couvreur, *Nat. Mat.* **2013**, *12*, 991-1003.

[28] D. Tarn, C. E. Ashley, M. Xue, E. C. Carnes, J. I. Zink, C. J. Brinker, *Acc. Chem. Res.* **2013**, *46*, 792-801.

[29] (a) E. Aznar, M. Oroval, Ll. Pascual, J. R. Muguía, R. Martínez-Máñez, F. Sancenón, *Chem. Rev.* **2016**, *116*, 561-718; (b) A. Agostini, L. Modragón, A. Bernardos, R. Martínez-Máñez, M. D. Marcos, F. Sancenón, J. Soto, A. Costero, C. Manguan-García, R. Perona, M. Moreno-Torres, R. Aparicio-Sanchis, J. R. Murguía, *Angew. Chem. Int. Ed.* **2012**, *51*, 10556-10560; (c) A. Agostini, L. Mondragón, C. Coll, E. Aznar, M. D. Marcos, R. Martínez-Máñez, F. Sancenón, J. Soto, E. Pérez-Payá, P. Amorós, *ChemOpen* **2012**, *1*, 17-20; (d) E. Aznar, R. Villalonga, C. Giménez, F. Sancenón, M. D. Marcos, R. Martínez-Máñez, P. Díez, J. M. Pingarrón, P. Amorós, *Chem. Commun.* **2013**, *49*, 6391-6393; (e) C. Giméenz, C. de la Torre, M. Gorbe, E. Aznar, F. Sancenón, J. R. Murguía, R. Martínez-Máñez, M. D. Marcos, P. Amorós, *Langmuir* **2015**, *31*, 3758-3762; (f) C. de la Torre, I. Casanova, G. Acosta, C. Coll, M. J. Moreno, F. Albericio, E. Aznar, R. Mangues, M. Royo, F. Sancenón, R. Martínez-Máñez, *Adv. Func. Mater.* **2015**, *25*, 687-695; (g) C. de la Torre, A. Agostini, L. Mondragón, M. Orzáez, F. Sancenón, R. Martínez-Máñez, M. D. Marcos, P. Amorós, E. Pérez-Payá, *Chem. Commun.* **2014**, *50*, 3184-3186; (h) E. Aznar, C. Coll, M. D. Marcos, R. Martínez-Máñez, F. Sancenón, J. Soto, P. Amorós, J. Cano, E. Ruiz, *Chem. Eur. J.* **2009**, *15*, 6877-6888: (i) E. Bringas, O. Köysüren, D. V. Quach, M. Mahmoudi, E. Aznar, J. D. Roehling, M. D. Marcos, R. Martínez-Máñez, P. Stroeve, *Chem. Commun.* **2012**, *48*, 5647-5649.

[30] (a) F. Sancenón, Ll. Pascual, M. Oroval, E. Aznar, R. Martínez-Máñez, *ChemOpen* **2015**, *4*, 418-437; (b) M. Oroval, E. Climent, C. Coll, R. Eritja, A. Aviñó, M. D. Marcos, F. Sancenón, R. Martínez-Máñez, P. Amorós, *Chem. Commun.* **2013**, *49*, 5480-5482; (c) Ll. Pascual, I. Baroja, E. Aznar, F. Sancenón, M. D. Marcos, J. R. Murguía, P. Amorós, K. Rurack, R. Martínez-Máñez, *Chem. Commun.* **2015**, *51*, 1414-1416.

[31] C. Giménez, E. Climent, E. Aznar, R. Martínez-Máñez, F. Sancenón, M. D. Marcos, P. Amorós, K. Rurack, *Angew. Chem. Int. Ed.* **2014**, *53*, 12629-12633.

[32] A. Llopis-Lorente, P. Diez, A. Sánchez, M. D. Marcos, F. Sancenón, P. Martínez-Ruíz, R. Villalonga, R. Martínez-Máñez, *Nat. Commun.* **2017**, *8*, 15511.

[33] J. Lu, M. Liong, Z. Li, J. I. Zink, F. Tamanoi, *Small* **2010**, *6*, 1794–1805.

[34] A. Baeza, M. Manzano, M. Colilla, M. Vallet-Regí, *Biomater. Sci.* **2016**, *4*, 803-813.

[35] J. M. Rosenholm, C. Sahlgren, M. Lindén, *Nanoscale* **2010**, *2,* 1870-1883.

[36] S. Poh, J. B. Lin, A. Panitch, *Biomacromolecules* **2015**, *16*, 1191−1200.

[37] A. Patel, K. Cholkar, A. K. Mitra, *Ther. Deliv*. **2014**, *5*, 337–365.

[38] B.Sung, C. Kim, M. H. Kim, *J. Colloid Interface Sci.* **2015**, *450*,

26-33.

[39] M. Witting, M. Molina, K. Obst, R. Plank, K. M. Eckl, H. C. Hennies, M. Calderón, W. Frieß, S. Hedtrich, *Nanomedicine*. **2015**, *11*, 1179-1187.

[40] E. Yu. I. Galiana, R. Martínez-Máñez, P. Stroeve, M. D. Marcos, E. Aznar, F. Sancenón, J. R. Murguía, P. Amorós, *Colloids Surf. B* **2015**, *135*, 652-660.

[41] K. Braun, A. Pochert, M. Lindén, M. Davoudi, A. Schimdtchen, R. Nordström, M. Malsmsten, *J. Colloid Interface Sci.* **2016**, *475*, 161-170.

[42] S. Shima, H. Sakai, *Agric. Biol. Chem.* **1977**, *41*, 1807- 1809.

[43] C. Zhou, P. Li, X. Qi, A. R. M. Sharif, Y. F. Poon, Y. Cao, M. W. Chang, S. Su Jan Leong, M. B. Chan-Park, *Biomaterials* **2011**, *32*, 2704-2712.

[44] I. L. Shih, M. H. Shen, Y. T. Van, *Bioresour. Technol*. **2006**, *97*, 1148-1159.

[45] S. Cabrera, J. El Haskouri, C. Guillem, J. Latorre, A. Beltrán, D. Beltrán, M. D. Marcos, P. Amorós, *Solid State Sci.* **2000**, *2*, 405-420.

[46] L. Mondragón, N. Mas, V. Ferragud, C. de la Torre, A. Agostini, R. Martínez-Máñez, F. Sancenón, P. Amorós, E. Pérez-Payá, M. Orzáez, *Chem. Eur. J.* **2014**, *20*, 5271-5281.

[47] N. J. Greenfield, *Nat. Protoc.* **2007**,*1,* 2876-2890.

[48] A. Mickan, D. Sarko, U. Haberkorn, W. Mier, *Curr. Pharm. Biotechnol.* **2014**, *15*, 200-209.

FULL PAPER

Two sets of MSNs loaded with safranin O or with C9h peptide and capped with ε-polylysine were prepared. A marked decrease in HeLa cell viability was observed when treated with C9h-loaded MSNs. Flow cytometry studies, showed the activation of apoptotic pathways in HeLa as a consequence of MSNs internalization, release of C9h peptide and disruption of caspase-9/PP2Acα interaction.

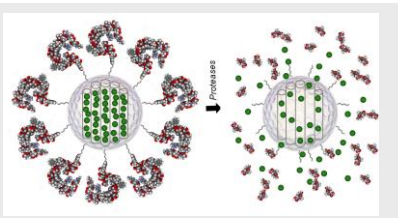

Cristina de la Torre, Leticia Domínguez-Berrocal, José R. Murguía, M. Dolores Marcos, Ramón Martínez-Máñez, Jerónimo Bravo,* and Félix Sancenón*

Page No. – Page No.

ε-polylysine-capped mesoporous silica nanoparticles as carrier of the C9h peptide to induce apoptosis in cancer cells